IEEE Access
Multidisciplinary | Rapid Review | Open Access Journal

Received April 27, 2018, accepted May 22, 2018, date of publication June 1, 2018, date of current version June 29, 2018.

Digital Object Identifier 10.1109/ACCESS.2018.2842797

Detection of Water Leakage in Underground Tunnels Using Corrected Intensity Data and 3D Point Cloud of Terrestrial Laser Scanning

TENG XU[1], LIJUN XU[1], (Senior Member, IEEE), XIAOLU LI[1], (Member, IEEE), AND JUNEN YAO[2]

[1]State Key Laboratory of Inertial Science and Technology, School of Instrument Science and Opto-Electronic Engineering, Beihang University, Beijing 100191, China
[2]Key Laboratory of Micro-Nano Measurement-Manipulation and Physics, School of Physics and Nuclear Energy Engineering, Ministry of Education, Beihang University, Beijing 100191, China

Corresponding authors: Lijun Xu (lijunxu@buaa.edu.cn) and Xiaolu Li (xiaoluli@buaa.edu.cn)

This work was supported in part by the National Natural Science Foundation of China under Grant 61671038 and Grant 61721091, in part by the Fundamental Research Funds for the Central Universities under Grant YWF-16-BJ-Y-54 and Grant YWF-17-BJ-Y-20, and in part by the Excellence Foundation of BUAA for the Ph.D. Students under Grant 2017058.

ABSTRACT Detection of water leakage is one of the most important regular tasks for underground tunnel inspection. In this paper, a new method is proposed for the water leakage detection in underground tunnels by using the corrected intensity data and 3-D point cloud of a terrestrial laser scanning (TLS) sensor. In the proposed method, the distance effect on the TLS intensity is first corrected based on a piecewise linear interpolation by using a reference target. Then, the distance-corrected intensity data are used to determine the surface roughness parameter that is specially considered to correct the incident angle effect. After corrections of distance and incident angle effects, the corrected intensity data are used to detect the water leakage regions in the underground tunnel. Finally, the appendages on the tunnel wall are removed by using the 3-D point cloud data to eliminate their influence on water leakage detection. To validate the feasibility of the proposed method, a case study in an underground tunnel in Beijing, China, was conducted by using a TLS sensor. Experimental results have demonstrated that the water leakage regions in the underground tunnel can be well extracted by using the corrected intensity data and 3-D point cloud, especially when the surface roughness is considered.

INDEX TERMS Intensity correction, terrestrial laser scanning, underground tunnel, water leakage, surface roughness.

I. INTRODUCTION

The underground tunnel has become one of the most ideal channels to reduce the distance of transport lines and relieve the increasing urban traffic challenges [1]. The regular inspection of an underground tunnel is necessary to ensure the safe operation and estimate the remaining life cycle, which can reduce the collapse risk of the underground tunnel. Water leakage is a typical phenomenon, which threatens the safety of operation for underground tunnel [2]. Therefore, detection of water leakage is one of the most important tasks of regular inspection for the underground tunnel.

There are some alternative methods to the water leakage detection of underground tunnels, such as the manual inspection method [3], [4], photogrammetry method [4], [5] and terrestrial laser scanning (TLS) method [6]. The manual inspection method is a conventional method of water leakage detection based on manual observations and judgments, which requires a large amount of manpower and investment of high cost [7]. Moreover, the accuracy of the conventional method is sensitive to personal judgments. The photogrammetry method obtains the digital image data of underground tunnel by using a Charge Coupled Device (CCD) camera and extracts the water leakage region from the digital image data. However, the photogrammetry method is a passive way and greatly influenced by the lighting conditions in the underground tunnel [8].

In particular, terrestrial laser scanning (TLS), an active remote sensing technique, is one of the most significant

means to acquire three-dimensional (3D) point data (x, y, z) of scanned targets [9]. Compared with other inspection methods, TLS has the advantages of high precision, high efficiency, and flexibility, which can obtain high-accuracy and high-density point cloud for regular inspection of underground tunnels [10]–[12]. As TLS is an active measurement method, it can work well without any external illumination and be suitable for the underground tunnel inspection [13]. Therefore, TLS shows its sufficient applicability and superiority in the underground tunnel inspection. In spite of this, detection of water leakage by using only the 3D point cloud of underground tunnels is still difficult for the reason that geometrical differences between the water leakage regions and non-leakage regions are slight. Besides 3D measurements for the geometrical structure of tunnels, TLS can record the intensity data of returned laser pulse scattered from scanned tunnels. Since the laser wavelength of TLS is commonly in the near-infrared band, the emitted light of TLS can be effectively absorbed by water [6]. The intensity values of water leakage regions are smaller than those of non-leakage regions. Therefore, TLS can be used to detect water leakage regions in underground tunnels by using 3D point cloud and intensity data.

However, raw intensity data of TLS are influenced by multiple factors, such as the system transmission factor, atmospheric factor, distance factor, incident angle factor and physical characteristics of scanned surfaces [14]–[17]. For raw intensity data obtained by the same TLS sensor at one project, the system transmission effect on TLS intensity data can be considered as a constant and the atmospheric effect can be ignored for a short-range TLS. Therefore, the distance and incident angle effects on TLS intensity data should be eliminated so that corrected intensity of TLS is only related to physical characteristics of scanned tunnels. The water leakage regions in underground tunnels can be extracted by using 3D point cloud and corrected intensity.

In the last few years, few researchers studied water leakage detection in underground tunnels using corrected intensity data from TLS. The only work we found from the literature is that done by Tan *et al.* [6]. However, he did not consider the surface roughness of scanned tunnels in correction of the intensity data. To improve the accuracy of water leakage detection, a novel method that considers and corrects the effect of surface roughness on the intensity data is proposed for water leakage detection in underground tunnels in this research. Our objective is to detect water leakage regions by using the corrected intensity data and 3D point cloud of a TLS sensor to ensure safe operation of underground tunnels. The contributions of the research include

(1) a new inspection method of underground tunnels is proposed to detect water leakage regions by combining the corrected intensity data and 3D point cloud of a TLS sensor;
(2) the surface roughness is specially considered in the correction of incident angle effect to improve the accuracy of water leakage detection;
(3) the appendages on the tunnel wall are removed from the water leakage regions by using the 3D point cloud data, which can eliminate their influence on water leakage detection. The feasibility of the inspection method is validated by experiments, and the results show that the water leakage regions in the underground tunnel can be well extracted.

The rest of this paper is organized as follows. The inspection method of water leakage regions was introduced in Section II. Data acquisition and preprocessing of underground tunnels was presented in Section III. Section IV provided and analyzed the experimental results. Section V summarized the conclusion of this research.

II. METHODOLOGY

A. FUNDAMENTALS ON TERRESTRIAL LASER SCANNING

The power of light backscattered from scanned objects in TLS follows the light detection and ranging (LiDAR) equation, which describes the relationship between received power and the emitted power. Therefore, the received power can be expressed as [18]

$$P_r = \frac{C\rho_\lambda \cos\theta}{R^2} \tag{1}$$

where C is a constant. P_r is the received power of a TLS sensor. R is the distance from the TLS sensor to a scanned object. θ is the incident angle between the incident light and the surface normal of the scanned object. ρ_λ is the surface reflectance of the scanned object at a certain laser wavelength λ. The recorded intensity I is commonly assumed as the amplitude of the received echo. Thus, we can obtain

$$I(R, \theta, \rho_\lambda) \propto P_r \propto \rho_\lambda R^{-2} \cos\theta \tag{2}$$

The intensity should be proportional to $\cos\theta$ and R^{-2} for scanned objects. However, the recorded intensity of many TLS sensors is not in a linear relationship with R^{-2} within the entire distance range. Furthermore, it is not sufficient to correct the incident angle effect for TLS intensity by using $\cos\theta$ because of that a large surface roughness or grain size makes scanned objects deviate significantly from the Lambertian model [19].

Since the distance and incident angle effects are independent from each other and can be eliminated separately [20], the TLS intensity data I can be expressed as

$$I(R, \theta, \rho_\lambda) = H_1(R) \cdot H_2(\theta) \cdot H_3(\rho_\lambda) \tag{3}$$

where $H_1(R)$, $H_2(\theta)$ and $H_3(\rho_\lambda)$ are the distance effect function, the incident angle effect function and the reflectance effect function, respectively.

In this research, a TLS sensor RIEGL VZ-400i was used to acquire the 3D point data and intensity data of the underground tunnel. The intensity I_{dB} of RIEGL VZ-400i is recorded in the unit of decibel (dB), which can be described as [21]

$$I_{\mathrm{dB}}(R, \theta, \rho_\lambda) = 10\log(I(R, \theta, \rho_\lambda)) = 10\log(\frac{P_r}{P_{th}}) \tag{4}$$

where P_r is the received power. P_{th} is the detection threshold power of the sensor, which is a constant. Therefore, substituting (3) into (4), we can obtain that

$$I_{\mathrm{dB}}(R, \theta, \rho_\lambda) = F_1(R) + F_2(\theta) + F_3(\rho_\lambda) \tag{5}$$

where

$$\begin{cases} F_1(R) = 10\log(H_1(R)) \\ F_2(\theta) = 10\log(H_2(\theta)) \\ F_3(\rho_\lambda) = 10\log(H_3(\rho_\lambda)) \end{cases} \tag{6}$$

$F_1(R)$, $F_2(\theta)$ and $F_3(\rho_\lambda)$ are decibel forms of $H_1(R)$, $H_2(\theta)$ and $H_3(\rho_\lambda)$, respectively.

B. INTENSITY CORRECTION

In reality, the recorded intensity of many TLS sensors usually shows different intensity-distance relationship rather than an ideal physical model (LiDAR equation) because of brightness reduction [22] and the receiver's defocusing [23] at near distance. Moreover, the distance effect functions of different types of TLS sensors are different from each other so that it is hardly to obtain a common distance effect function for different types of TLS sensors. $F_1(R)$ can be approximately considered as a linear function within a small distance. Therefore, the distance effect can be eliminated by using a piecewise linear interpolation method based on a reference target in this paper, which makes that the estimation of $F_1(R)$ can be avoidable.

If a reference target with the reflectance of ρ_s is scanned by a TLS sensor under a fixed incidence angle of θ_s, the intensity data are collected at different distances. The distance value R_s should meet as

$$R_s = \{R_0, R_1, \cdots, R_n\}, \quad \text{and } R_0 < R_1 \cdots < R_i \cdots < R_n \tag{7}$$

The recorded intensity is denoted as $I_{\mathrm{dB}}(R_x, \theta_x, \rho)$ of a scanned object with the reflectance of ρ at the distance of R_x and the incident angle of θ_x. When the distance value R_x meets the following relationship as

$$R_i < R_x < R_{i+1}, \quad i = 1, 2, \cdots n-1 \tag{8}$$

The intensity value $I_{\mathrm{dB}}(R_x, \theta_s, \rho_s)$ can be obtained by means of piecewise linear interpolation, i.e.,

$$\begin{aligned} I_{\mathrm{dB}}(R_x, \theta_s, \rho_s) &= F_1(R_x) + F_2(\theta_s) + F_3(\rho_s) \\ &= \frac{I_{\mathrm{dB}}(R_{i+1}, \theta_s, \rho_s) - I_{\mathrm{dB}}(R_i, \theta_s, \rho_s)}{R_{i+1} - R_i} \\ &\quad \times (R_x - R_i) + I_{\mathrm{dB}}(R_i, \theta_s, \rho_s) \end{aligned} \tag{9}$$

where $I_{\mathrm{dB}}(R_s, \theta_s, \rho_s)$ ($R_s = \{R_0, R_1, \cdots, R_n\}$) is denoted as the reference intensity.

Combined with (9) and (5), we can obtain that

$$\begin{aligned} &I_{\mathrm{dB}}(R_x, \theta_x, \rho) - I_{\mathrm{dB}}(R_x, \theta_s, \rho_s) \\ &= F_1(R_x) + F_2(\theta_x) + F_3(\rho) - (F_1(R_x) + F_2(\theta_s) + F_3(\rho_s)) \\ &= F_2(\theta_x) + F_3(\rho) - F_2(\theta_s) - F_3(\rho_s) \end{aligned} \tag{10}$$

Thus, the distance corrected intensity $I_{dis}(R_x, \theta_x, \rho)$ can be obtained as

$$\begin{aligned} I_{dis}(R_x, \theta_x, \rho) &= F_2(\theta_x) + F_3(\rho) \\ &= I_{\mathrm{dB}}(R_x, \theta_x, \rho) - I_{\mathrm{dB}}(R_x, \theta_s, \rho_s) + F_2(\theta_s) + F_3(\rho_s) \end{aligned} \tag{11}$$

As the incident angle of θ_s and the reflectance of ρ_s are fixed, $F_2(\theta_s)$ and $F_3(\rho_s)$ are constants. Equation (11) can be simplified as

$$I_{dis}(R_x, \theta_x, \rho) = I_{\mathrm{dB}}(R_x, \theta_x, \rho) - I_{\mathrm{dB}}(R_x, \theta_s, \rho_s) + K_0 \tag{12}$$

where $K_0 = F_2(\theta_s) + F_3(\rho_s)$. From (12), we can know that the distance corrected intensity $I_{dis}(R_x, \theta_x, \rho)$ is only related to the incident angle effect and the reflectance of scanned targets.

After the distance effect is eliminated, the incident angle effect on the distance corrected intensity $I_{dis}(R_x, \theta_x, \rho)$ should be eliminated to make that TLS intensity is only related to the reflectance of scanned targets. Perfect diffuse scattering from scanned targets, e.g., the Lambertian reflector, has been widely used to eliminate the incident angle effect. However, some scanned targets with rough surface deviate significantly from the Lambertian reflector. Oren-Nayar model well addresses this issue proposing a new model of faceted surfaces, which is a physical reflectivity model to describe the surface roughness [24]. Compared with the Lambertian model, the Oren-Nayar model is more realistic considering individual roughness and micro structure. It is more consistent with the real laser reflection conditions of natural surfaces and can accurately and quantitatively simulate the luminance from natural surfaces. Thus, the micro-faceted surface reflectance model of Oren–Nayar was used to correct the incident angle effect in this study. In TLS, the incident and reflected lights are coincident and the Oren-Nayar model can be simplified as [25]

$$L_r = L_i \cos\theta (A + B \sin\theta \tan\theta) \tag{13}$$

$$A = 1 - 0.5\frac{\sigma_{slope}^2}{\sigma_{slope}^2 + 0.33}, \quad B = 0.45\frac{\sigma_{slope}^2}{\sigma_{slope}^2 + 0.09} \tag{14}$$

where L_i and L_r are the radiance of the incident light shot on the scanned surface and radiance of the reflected light from the scanned surface, respectively. The surface roughness parameter $\sigma \in (0, \pi/2)$ is the standard deviation of the slope angle distribution in radians. For flat surfaces without facet variation (i.e. σ is equal to 0°), the Oren-Nayar model is equal to the Lambertian model. Based on the Oren-Nayar model, the function of the incident angle effect can be described as

$$\begin{aligned} F_2(\theta_x) = 10\log(\cos\theta_x (1 - 0.5\frac{\sigma_{slope}^2}{\sigma_{slope}^2 + 0.33} \\ + 0.45\frac{\sigma_{slope}^2}{\sigma_{slope}^2 + 0.09} \sin\theta_x \tan\theta_x)). \end{aligned} \tag{15}$$

Substituting (15) into (11), we can obtain the corrected intensity I_c of scanned objects as follow

$$\begin{aligned} I_c &= K_0 + I_{dis}(R_x, \theta_x, \rho) - F_2(\theta_x) \\ &= K_0 + I_{\mathrm{dB}}(R_x, \theta_x, \rho) - I_{\mathrm{dB}}(R_x, \theta_s, \rho_s) - 10\log[\cos\theta_x \\ &\quad \times (1 - 0.5\frac{\sigma_{slope}^2}{\sigma_{slope}^2 + 0.33} \\ &\quad + 0.45\frac{\sigma_{slope}^2}{\sigma_{slope}^2 + 0.09}\sin\theta_x \tan\theta_x)] \end{aligned} \tag{16}$$

After the corrections of the distance and incident effects, the corrected intensity I_c merely depends on the reflectance of scanned objects.

C. DETERMINATION OF SURFACE ROUGHNESS PARAMETER

In order to find the optimal value of surface roughness parameter σ_{slope}, the detail steps are given as follows. Firstly, we manually select some small homogeneous regions on the surface of scanned objects and calculate the mean intensity values $\bar{I}_{\mathrm{dB}}(\bar{R}_m, \bar{\theta}_m, \rho, \sigma_{slope})$ (where m and M are the serial number and the total number of the selected homogeneous regions, m=1, 2, …, M) of each homogeneous region. Then, according to (12), the distance effect is corrected for all homogenous regions, and the distance corrected intensity $\bar{I}_{dis}(\bar{R}_m, \bar{\theta}_m, \rho, \sigma_{slope})$ can be obtained. Finally, the incident angle effect on the intensity $\bar{I}_{dis}(\bar{R}_m, \bar{\theta}_m, \rho, \sigma_{slope})$ is eliminated through (16) with the parameter σ_{slope} varied from 1° to 90° in a step interval of 1°, and the corrected intensity are denoted as $\bar{I}_c(\bar{R}_m, \bar{\theta}_m, \rho, \sigma_{slope})$.

$$O(\sigma_{slope}) = \sqrt{\frac{\sum_{m=1}^{m=M}\sum_{n=m}^{n=M}\left|\bar{I}_c(R_m, \theta_m, \rho, \sigma_{slope}) - \bar{I}_c(R_n, \theta_n, \rho, \sigma_{slope})\right|}{M \times (M+1)/2}} \tag{17}$$

$$(\sigma_{slope})_{optimal} = \min_{0 \le \sigma_{slope} < \frac{\pi}{2}} O(\sigma_{slope}) \tag{18}$$

where m and n are both the serial numbers of the homogeneous regions. Once the optimal value of surface roughness parameter σ_{slope} is determined according to (18), it is substituted into (16) to correct the intensity data of the collected dataset.

D. WATER LEAKAGE DETECTION

In the proposed method, 3D point cloud data and intensity data of the underground tunnel are acquired by a TLS sensor, which are processed to extract water leakage regions in the underground tunnel. The specific processing flow of the proposed method is shown in Fig. 1.

First of all, the dataset of 3D points (x, y, z) are filtered to remove the noise points based on the nearest neighbor search approach, where the diameter of the search neighbor and the minimum number of points in the neighbor are 0.05 m and 5.

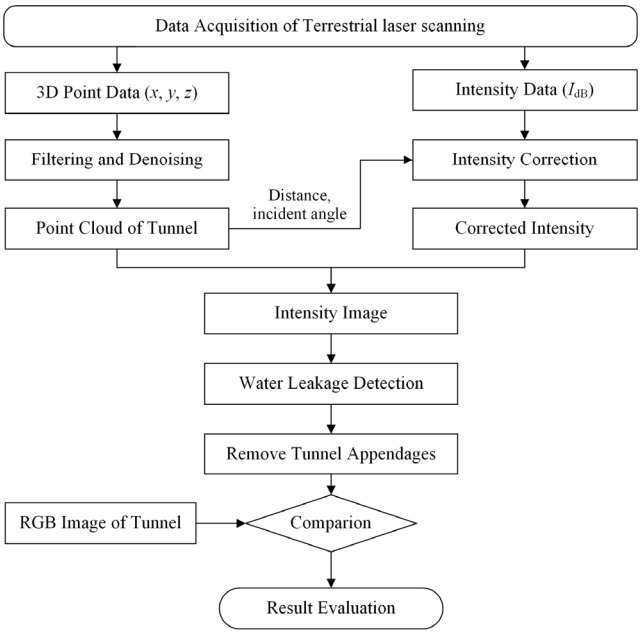

FIGURE 1. Flow chart of water leakage detection by using corrected intensity data.

When the number of points in the neighbor of a seed point is less than 5, the point is judged as a noise point and should be removed. The distance effect and incident angle effect corrections are performed to obtain the corrected intensity, which is merely related to the reflectance of the tunnel wall. Then, combined with the obtained 3D point cloud and the corresponding corrected intensity data, the intensity image of the tunnel is formed. Finally, water leakage regions in the tunnel can be detected from the corrected intensity data by using a threshold method. The appendages (pipe, cable box, etc.) on the tunnel wall are removed based on the plane fitting method by using 3D point cloud, which can eliminate the influence of the appendages on the water leakage detection.

In order to extract the water leakage regions in the tunnel, the intensity threshold value to separate water leakage and non-water leakage regions should be determined. In this paper, non-water leakage regions in the tunnel are selected, and then the mean value ($\bar{I}_{c0}$) and standard deviation (Std_Dev) are calculated as follow

$$\begin{cases} \bar{I}_{c0} = (\sum_{n=1}^{N} I_c^{(n)})/N \\ \mathrm{Std\_Dev} = \sqrt{\frac{1}{N} \times \sum_{n=1}^{N} (I_c^{(n)} - \bar{I}_{c0})} \end{cases} \tag{19}$$

where n and N are the serial number and the total number of points from the selected regions, respectively.

According to the three-sigma criterion, $\bar{I}_{c0} - 3 \times \mathrm{Std\_Dev}$ is the lower limit of the intensity value at a point that is not in the water leakage region. Since the intensity values in water leakage regions are lower than those in the non-leakage regions, the value of $\bar{I}_{c0} - 3 \times \mathrm{Std\_Dev}$ is selected

as the threshold to determine whether the point is in water leakage region or not. When the intensity value is larger than $\bar{I}_{c0} - 3 \times \text{Std\_Dev}$, it is judged as non-water leakage regions, otherwise it is judged as water leakage regions. Therefore, water leakage and non-water leakage regions can be separated from each other, and the water leakage regions in the underground tunnel are detected through (20).

$$\begin{cases} if\,(I_c >= \bar{I}_{c0} - 3 \times \text{Std\_Dev}), & non-water\ leakage\ point \\ otherwise, & water\ leakage\ point \end{cases} \tag{20}$$

As the intensity values of tunnel appendages are close to the intensity values of water leakage regions, the tunnel appendages seriously affect the detection of water leakage regions. These appendages attached on the tunnel wall should be removed to eliminate their influence on the water leakage detection. Since the tunnel wall is approximately flat, the plane fitting method by using 3D point cloud is applied to remove these tunnel appendages in this paper. To improve the fitting effect and remove the tunnel appendages well, the tunnel wall is divided into some parts. 3D points in each part are used for a local plane fitting through (21)

$$A_i x + B_i y + C_i z = D_i, (x, y, z) \in \mathbf{\Omega}_i \quad \text{and } i = 1, 2, \cdots, K \tag{21}$$

where (x, y, z) are coordinates of 3D points, A_i, B_i, C_i, D_i are the coefficients of the ith plane. $\mathbf{\Omega}_i$ is the point set of the ith part of the tunnel wall.

Assume that coordinates of any point P_i in the point set $\mathbf{\Omega}_i$ are (x_i, y_i, z_i). Thus, the distance d_{P_i} between point P_i and the plane can be expressed as

$$d_{P_i} = \frac{|A_i * x_i + B_i * y_i + C_i * z_i = D_i|}{\sqrt{A_i^2 + B_i^2 + C_i^2}}, \quad (x_i, y_i, z_i) \in \mathbf{\Omega}_i \tag{22}$$

Combined with 3D geometrical information of the tunnel wall, a threshold δ is determined to distinguish points of the tunnel appendages and the tunnel wall.

$$\begin{cases} if\,(d_{P_i} >= \delta), & P_i \in tunnelappendages \\ otherwise, & P_i \in tunnelwall \end{cases} \tag{23}$$

where the threshold δ is manually set as 0.03 m. Thus, according to (23), these appendages can be removed from the tunnel wall.

III. EXPERIMENTS

In this section, two different types of experiments were conducted by using the TLS sensor RIEGL VZ-400i. First, the distance experiment focused on the correction of the distance effect on TLS intensity. Second, an experiment for water leakage detection was carried out to extract water leakage regions in the scanned underground tunnel.

To obtain the reference intensity $I_{\text{dB}}(R_s, \theta_s, \rho_s)$ in (9), a reference target with a size of 60 cm $\times$ 60 cm, the reflectance of 30% (@1550 nm) was scanned by using a TLS sensor at different distances. All the scans were collected by the sensor at the condition that the incident angle of the reference target was a constant during the data collection process. The data acquisition in the distance experiment was performed with the 1 m interval from 4 m to 35 m. The TLS sensor used in this study is the terrestrial laser scanner, which has a near-infrared (1550 nm) laser beam with the divergence of 0.35 mrad and a range accuracy of 5 mm (one sigma @ 100 m) [26].

In the experiment of water leakage detection, an underground tunnel at Fengtai District, Beijing, China (39.808664N, 116.308112E) was scanned by the TLS sensor, which was utilized to acquire 3D point cloud data and intensity data of the tunnel. Figure 2 is point cloud of the underground tunnel, which is colored with raw intensity. In this research, we select a profile of the underground tunnel (shown in the red box of Fig. 2) as the investigated object to extract water leakage regions.

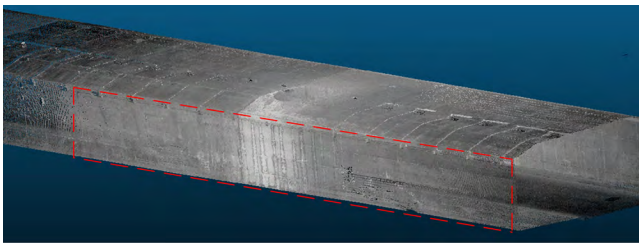

FIGURE 2. 3D point cloud data obtained by a TLS sensor (RIEGL VZ400i).

IV. RESULTS

A. RESULTS OF INTENSITY CORRECTION

To eliminate the distance effect on raw intensity data, the distance correction should be completed firstly. Variations of raw intensity I_{dB} and ΔI_{dB} with distance for the reference target with the reflectance of 30% are shown in Fig. 3.

The mean of raw intensity first increases with distance and reaches the maximum value at about 10 m. Then it constantly decreases with distance thereafter (as shown in Fig. 3(a)). The reason is that the system transmission factor such as the brightness reducer and receiver optics' defocusing, severely influences on the raw intensity at near distance. However, at far distance, the distance effect becomes the main factor on the raw intensity. Within the entire distance range, we can know that the standard deviations of intensity data are all less than 0.5 dB and the maximum and minimum of ΔI_{dB} is 0.62 dB and -0.40 dB (as shown in Fig. 3(b)), which indicates that the raw intensity changes slightly within the interval of 1 m. Thus, the distance effect can be corrected by using the linear interpolation method through (9) in this paper.

To obtain the surface roughness of the underground tunnel, we manually selected 20 small homogenous regions on the tunnel wall to reduce the random measurement error of the TLS sensor. To obtain enough points and make the selected regions homogenous, the diameter of the selected regions was set as 3cm here. The distributions of distances and incidence angles are shown in Fig. 4.

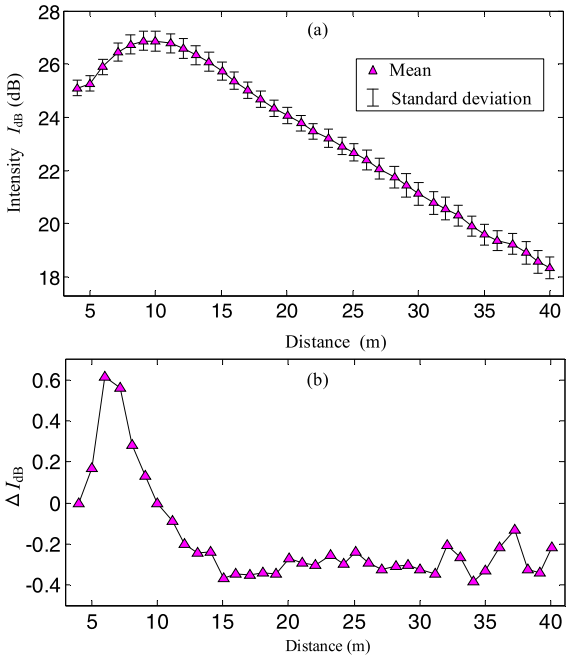

FIGURE 3. Variations of intensity I_{dB} and ΔI_{dB} with distance for the reference target at a fixed incident angle. (a) raw intensity I_{dB} varies with distance, (b) ΔI_{dB} varies with distance (where $\Delta I_{dB}(R_{i+1}) = I_{dB}(R_{i+1}) - I_{dB}(R_i)$, $R_{i+1} - R_i = 1$ m, $R_i = 4, 5, \ldots, 35$ m).

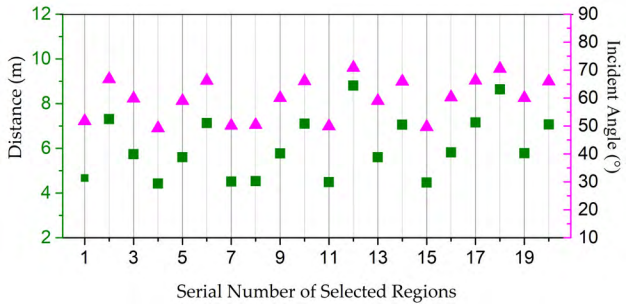

FIGURE 4. Distribution of distances and incidence angles of 20 homogeneously selected regions

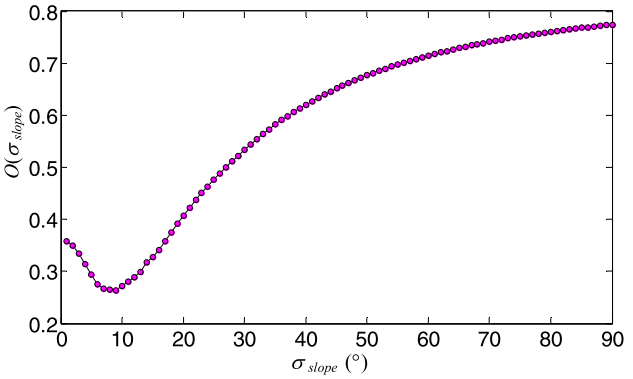

FIGURE 5. Variation of the objective function $O(\sigma_{slope})$ with the tunnel surface roughness.

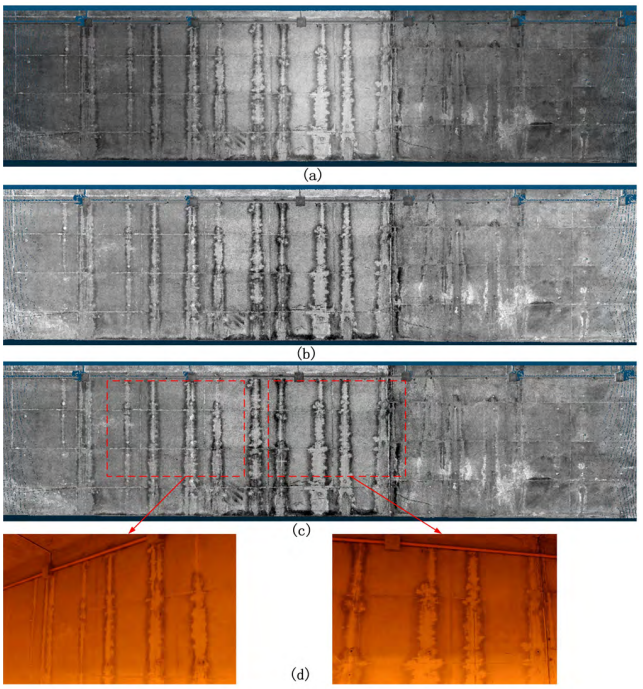

FIGURE 6. Intensity images of the tunnel wall before and after intensity correction, as compared with corresponding RGB images, (a) Raw intensity image, (b) Intensity image after the Lambertian model-based correction, (c) Intensity image after the Oren-Nayar model-based correction, (d) RGB images captured by a CCD camera.

According to (17), the objective function $O(\sigma_{slope})$ at different surface roughness parameter can be calculated, as shown in Fig. 5. From Fig. 5, we can see that the value of the objective function first reduces with the surface roughness parameter σ_{slope} and reaches the maximum when the value of σ_{slope} is 9°. Then it constantly increases with σ_{slope} thereafter. Therefore, the optimal value of the surface roughness parameter σ_{slope} is determined as 9°.

B. RESULTS OF WATER LEAKAGE DETECTION

The intensity images of the underground tunnel before and after intensity correction obtained by the TLS sensor, and RGB images captured by a CCD camera are shown in Fig. 6.

From Fig. 6(a), we can see that due to the distance effect and incidence angle effect on the raw intensity, the middle part of the intensity image is brighter (the values of the raw intensity are larger), and the two edge parts of the image are darker (the values of the raw intensity are smaller). The piecewise linear interpolation method by using the reference target is used to correct the distance effect of the raw intensity. Then, the distance corrected intensity data are further corrected to eliminate the incidence angle effect by using the Lambertian model and Oren-Nayar model, respectively. The corrected intensity images after the two model-based corrections are shown in Fig. 6 (b) and (c), respectively. Compared with the distribution range of the raw intensity data, the distribution ranges of the corrected intensity data of the tunnel reduce from [15.61 dB, 31.74 dB] to [−3.56 dB, 9.88 dB]

(Lambertian model-based correction) and [−4.08 dB, 9.51 dB] (Oren-Nayar model-based correction). After intensity correction, the distributions of the intensity data are more concentrated. The intensity values of the same target are closer to each other, and the differences of the intensity values of different targets are bigger, which can well suppress the phenomenon of ''different objects with the same spectrum''. Furthermore, after intensity corrections, the intensity values of the water leakage regions are obviously smaller than those of non-water leakage regions. Thus, the water leakage regions in the intensity images can be easily extracted by using the corrected intensity data.

In order to obtain the threshold value between water leakage and non-water leakage regions, some non-water leakage regions are selected from the tunnel wall. The distributions of the raw and corrected intensity data of the selected non-water leakage regions are shown in Fig. 7. The distributions of the intensity data corrected by the Lambertian model and Oren-Nayar model are both more concentrated than that of the raw intensity data. Furthermore, from the statistical results in Table 1, we can also know that the standard deviations (Std.) of the raw intensity data, corrected intensity data by using the Lambertian model and Oren-Nayar model are 0.50 dB, 0.44 dB and 0.38 dB, respectively, which indicates that the correction performance using the Oren-Nayar model is better than that using the Lambertian model. For the raw intensity image, the intensity images after the Lambertian model-based correction and Oren-Nayar model-based correction, the threshold values of them between water leakage and non-water leakage regions are 20.02 dB, 0.75 dB and 0.45 dB, respectively.

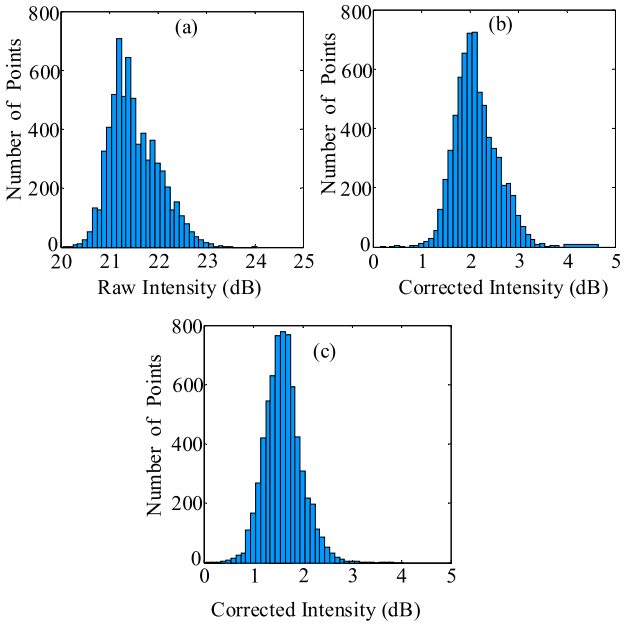

FIGURE 7. Histograms of raw and corrected intensity data of non-water leakage regions on the underground tunnel wall. (a) histogram of raw intensity data, (b) histogram of intensity data corrected by the Lambertian model, (c) histogram of intensity data corrected by Oren-Nayar model.

TABLE 1. Statistical results of the intensity distributions for the non-water leakage regions of the underground tunnel.

Statistical Results	Raw Intensity	Corrected Intensity by Lambertian Model	Corrected Intensity by Oren-Nayar Model
Mean	21.52 dB	2.07 dB	1.59 dB
Std.	0.50 dB	0.44 dB	0.38 dB

As mentioned above, the threshold values are used to distinguish the water leakage and non-water leakage regions so that water leakage regions on the tunnel wall can be well detected. The water leakage regions detected from intensity images are shown in the blue parts of Fig. 8.

Due to the distance and incident angle effects on the raw intensity data, the detection of water leakage regions is very poor by using the raw intensity data directly and most water leakage regions cannot be detected, as shown in Fig. 8(a). After the distance and incident angle effects are eliminated, the corrected intensity is only related to the reflectance of the tunnel wall. Therefore, the water leakage regions on the tunnel wall can be accurately detected by using the corrected intensity data, as shown in Fig. 8(b) and (c). Furthermore, compared with the detection of water leakage regions from intensity image after Oren-Nayar model-based correction, some water leakage regions cannot be accurately detected from intensity image after Lambertian model-based correction, as shown in the red boxes of Fig. 8(b) and (c). The reason is that the influence of the surface roughness of the tunnel wall on the raw intensity is not considered during the incident angle effect correction by using the Lambertian model. Thus, the missed detection exists in water leakage detection from intensity image after Lambertian model-based correction.

To extract the water leakage regions, the binarization for the intensity image after the Oren-Nayar model-based correction is performed. The water leakage regions extracted from intensity image can be obtained as shown in black parts of Fig. 9. From Fig. 9(a), we can see that the appendages mix with the extracted water leakage regions, which seriously affects the judgment of the water leakage regions on the tunnel wall. Therefore, the tunnel appendages in Fig. 9(a) were removed based on the plane fitting method by using 3D point cloud. The binary image after removal of tunnel appendages is shown in Fig. 9(b), which still has some isolated points. It may be caused by the system measurement error or contaminants attached on the tunnel wall. To remove these isolated points mixed with water leakage regions, a median filtering was performed on Fig. 9(b). The binary image after further median filtering is shown in Fig. 9(c). These isolated points had been nearly filtered after the median filtering, which eliminated the influence of tunnel appendages on water leakage detection. Figure 9(c) shows that there are 211583 pixels for the water leakage regions, and the total pixels of the intensity image is 1965280. Thus, the rate of water leakage regions in the tunnel is $211583/1965280 \times 100\% = 10.76\%$.

It should be noted that the results we have obtained are only on whether water leakage exists in a certain

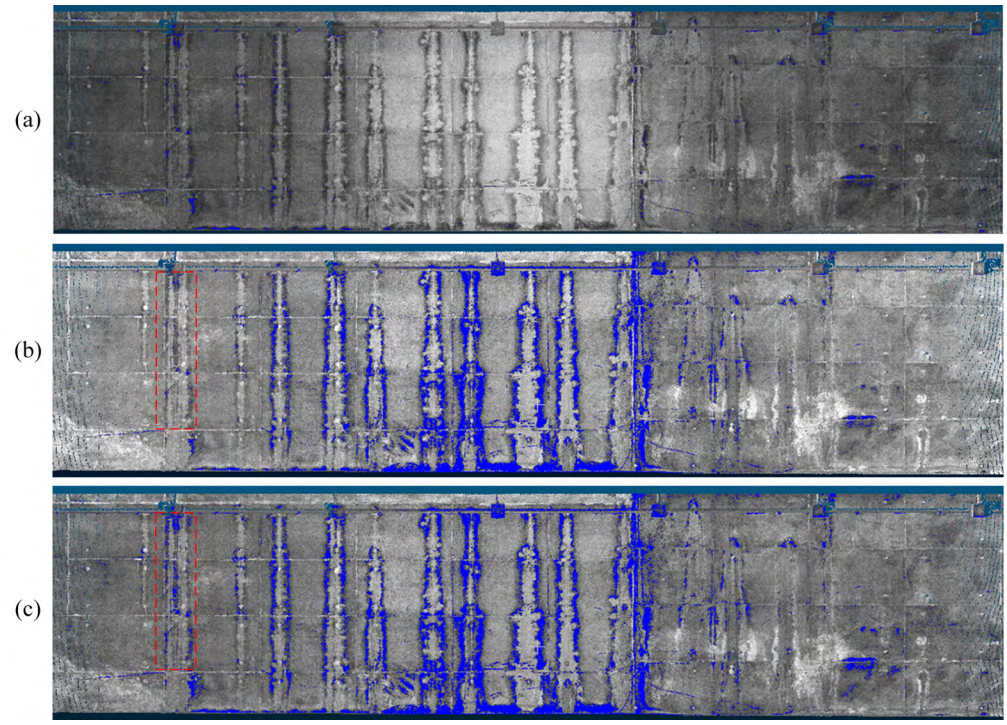

FIGURE 8. Detection of water leakage regions (blue parts) using the raw and corrected intensity data. (a) Results detected from raw intensity data, (b) results detected from intensity data corrected by Lambertian model, (c) results detected from intensity data corrected by Oren-Nayar model.

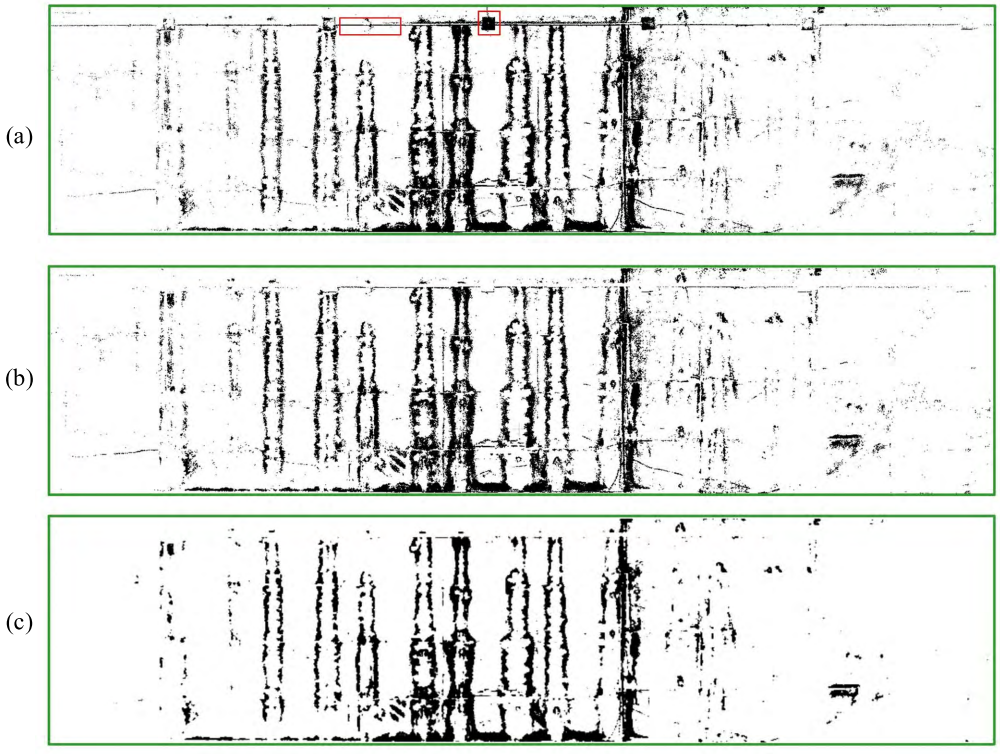

FIGURE 9. Results of water leakage spots extraction. (a) Binary image of intensity data corrected by Oren-Nayar model, (b) Binary image after removal of tunnel appendages, (c) Binary image after further median filtering.

region on the tunnel wall. As it is hard to determine and measure the in-situ water content of the tunnel wall, the results are still qualitative. In the future, further studies are required to establish a quantitative model to infer water content of the tunnel wall from corrected intensity data.

V. CONCLUSIONS

In this research, we proposed a novel method to detect water leakage in underground tunnels by using the corrected intensity data and 3D point cloud of the TLS sensor. From the experimental results, it can be seen that

(1) After corrections of the distance and incident angle effects on TLS raw intensity, the corrected intensity is merely and well related to the reflectance of the tunnel wall.

(2) Water leakage regions in the underground tunnel can be well extracted by using the corrected intensity data of TLS, when compared with the RGB images. As the surface roughness parameter is considered in the Oren-Nayar model during intensity correction, the results of water leakage detection using Oren-Nayar model is better than those using the Lambertian model.

(3) By using the 3D point cloud data, the tunnel appendages were removed from the water leakage regions extracted from the corrected intensity data, which had completely eliminated the influence of tunnel appendages on water leakage detection.

Obviously, the proposed method can also be applied in many other scenes such as water leakage detection for metro, building roofs, and bridges without the need of modification to the method.

ACKNOWLEDGMENT

The authors would like to gratefully acknowledge the RIEGL agency (Five-star Electronic Technology Company Limited) who provided them the instrument RIEGL VZ-400i.

REFERENCES

[1] Y.-J. Cheng, W. Qiu, and J. Lei, "Application of terrestrial laser scanning in tunnel inspection," *Electron. J. Geotech. Eng.*, vol. 21, no. 12, pp. 4683–4688, 2016.

[2] S. C. Li, J. Wu, Z. H. Xu, and L. P. Li, "Unascertained measure model of water and mud inrush risk evaluation in karst tunnels and its engineering application," *J. Civil Eng.*, vol. 21, no. 4, pp. 1170–1182, 2017.

[3] R. Montero, J. G. Victores, S. Martínez, A. Jardón, and C. Balaguer, "Past, present and future of robotic tunnel inspection," *Automat. Construct.*, vol. 59, no. 1, pp. 99–112, 2015.

[4] T. Asakura and Y. Kojima, "Tunnel maintenance in Japan," *Tunnelling Underground Space Technol.*, vol. 18, nos. 2–3, pp. 161–169, 2003.

[5] K. Makantasis, E. Protopapadakis, A. Doulamis, N. Doulamis, and C. Loupos, "Deep convolutional neural networks for efficient vision based tunnel inspection," in *Proc. ICCP*, Cluj-Napoca, Romania, Sep. 2015, pp. 335–342.

[6] K. Tan, X. Cheng, Q. Ju, and S. Wu, "Correction of mobile TLS intensity data for water leakage spots detection in metro tunnels," *IEEE Geosci. Remote Sens. Lett.*, vol. 13, no. 11, pp. 1711–1715, Nov. 2016.

[7] C. Balaguer, R. Montero, J. G. Victores, S. Martínez, and A. Jardón, "Towards fully automated tunnel inspection: A survey and future trends," in *Proc. 31st Int. Symp. Automat. Robot. Construct. Mining*, Sydney, NSW, Australia, 2014, pp. 19–33.

[8] T. Nuttens *et al.*, "High resolution terrestrial laser scanning for tunnel deformation measurements," in *Proc. FIG*, Sydney, NSW, Australia, 2010, pp. 11–16.

[9] J. Kasperski, C. Delacourt, P. Allemand, P. Potherat, M. Jaud, and E. Varrel, "Application of a terrestrial laser scanner (TLS) to the study of the Séchilienne landslide (Isère, France)," *Remote Sens.*, vol. 2, no. 12, pp. 2785–2802, 2010.

[10] S. Y. W. Lam, "Application of terrestrial laser scanning methodology in geometric tolerances analysis of tunnel structures," *Tunnelling Underground Space Technol.*, vol. 21, no. 3, p. 410, 2006.

[11] Z. Kang, L. Zhang, L. Tuo, B. Wang, and J. Chen, "Continuous extraction of subway tunnel cross sections based on terrestrial point clouds," *Remote Sens.*, vol. 6, no. 1, pp. 857–879, 2014.

[12] K. Tan, X. Cheng, and Q. Ju, "Combining mobile terrestrial laser scanning geometric and radiometric data to eliminate accessories in circular metro tunnels," *J. Appl. Remote Sens.*, vol. 10, no. 3, p. 030503, 2016.

[13] V. Gikas, "Three-dimensional laser scanning for geometry documentation and construction management of highway tunnels during excavation," *Sensors*, vol. 12, no. 8, pp. 11249–11270, 2012.

[14] T. Xu, L. Xu, B. Yang, X. Li, and J. Yao, "Terrestrial laser scanning intensity correction by piecewise fitting and overlap-driven adjustment," *Remote Sens.*, vol. 9, no. 11, p. 1090, 2017.

[15] A. G. Kashani, M. J. Olsen, C. E. Parrish, and N. Wilson, "A review of LiDAR radiometric processing: From ad hoc intensity correction to rigorous radiometric calibration," *Sensors*, vol. 15, no. 11, pp. 28099–28128, 2015.

[16] S. Kaasalainen, A. Jaakkola, M. Kaasalainen, A. Krooks, and A. Kukko, "Analysis of incidence angle and distance effects on terrestrial laser scanner intensity: Search for correction methods," *Remote Sens.*, vol. 3, no. 10, pp. 2207–2221, 2011.

[17] K. Tan, K. Liu, and X. Cheng, "An empirical method in correcting specular highlight phenomenon in TLS intensity data," *IEEE Access*, vol. 4, pp. 9821–9827, 2016.

[18] W. Wagner, "Radiometric calibration of small-footprint full-waveform airborne laser scanner measurements: Basic physical concepts," *J. Photogramm. Remote Sens.*, vol. 65, no. 6, pp. 505–513, 2010.

[19] K. Tan, X. Cheng, and X. Cheng, "Modeling hemispherical reflectance for natural surfaces based on terrestrial laser scanning backscattered intensity data," *Opt. Express*, vol. 24, no. 20, pp. 22971–22988, 2016.

[20] A. Krooks, S. Kaasalainen, T. Hakala, and O. Nevalainen, "Correction of intensity incidence angle effect in terrestrial laser scanning," *Ann. Photogramm. Remote Sens. Spatial Inf. Sci.*, vol. 2, pp. 145–150, Nov. 2013.

[21] M. Pfennigbauer and A. Ullrich, "Improving quality of laser scanning data acquisition through calibrated amplitude and pulse deviation measurement," *Proc. SPIE*, vol. 7684, p. 76841F, Apr. 2010.

[22] S. Kaasalainen *et al.*, "Brightness measurements and calibration with airborne and terrestrial laser scanners," *IEEE Trans. Geosci. Remote Sens.*, vol. 46, no. 2, pp. 528–534, Feb. 2008.

[23] G. Biavati, G. D. Donfrancesco, F. Cairo, and D. G. Feist, "Correction scheme for close-range lidar returns," *Appl. Opt.*, vol. 50, no. 30, pp. 5872–5882, 2011.

[24] M. Oren and S. K. Nayar, "Generalization of Lambert's reflectance model," in *Proc. SIGGRAPH*, Orlando, FL, USA, 1994, pp. 239–246.

[25] D. Carrea, A. Abellan, F. Humair, B. Matasci, M.-H. Derron, and M. Jaboyedoff, "Correction of terrestrial LiDAR intensity channel using Oren–Nayar reflectance model: An application to lithological differentiation," *J. Photogramm. Remote Sens.*, vol. 113, pp. 17–29, Mar. 2016.

[26] RIEGL Laser Measurement Systems GmbH, Horn, Austria. *Datasheet RIEGL VZ-400i*. Accessed: Apr. 2018. [Online]. Available: http://www.riegl.com/uploads/tx_pxprieggldownloads/RIEGL_VZ-400i_Datasheet_2017-12-18.pdf

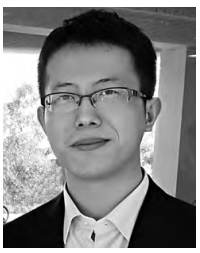

TENG XU received the B.Sc. and M.Eng. degrees in instrument science and technology from Beihang University, Beijing, China, in 2012 and 2014, respectively, where he is currently pursuing the Ph.D. degree with the School of Instrument Science and Opto-Electronic Engineering.

His current research interests include positioning error analysis and intensity correction and its application of LiDAR.

LIJUN XU (M'04–SM'04) received the B.Sc., M.Eng., and Ph.D. degrees in electrical engineering and instrumentation from Tianjin University, Tianjin, China, in 1990, 1993, and 1996, respectively. From 1997 to 2001, he was an Associate Professor with the School of Electrical Engineering and Automation, Tianjin University. From 2002 to 2004, he was a Research Fellow with the University of Greenwich, Chatham, U.K., and the University of Kent, Canterbury, U.K. From 2004 to 2006, he was a Higher Scientific Officer with the Department of Physics, Institute of Cancer Research, University of London, London, U.K. He is currently the Dean and also a Professor with the School of Instrument Science and Opto-Electronic Engineering, Beihang University, Beijing, China. He has authored or co-authored over 250 publications. His current research interests include tomographic imaging, scanning imaging, and dynamic process monitoring.

Dr. Xu received the National Science Fund for Distinguished Young Scholars and the Ministry of Education Technology Invention Award (first class) in 2012, and the China Instrument Society Science and Technology Award (1st class) in 2014. He was nominated as a Chang-Jiang Scholars Program Professor by the Ministry of Education of China in 2014.

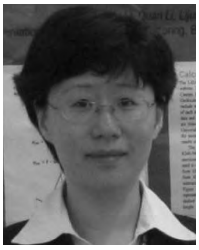

XIAOLU LI received the Ph.D. degree in physical electronics from Beihang University in 2009. She is currently an Associate Professor with the School of Instrumentation and Opto-Electronic Engineering, Beihang University. She has published over 70 referred papers, such as the *Remote Sensing Letters*, the IEEE TRANSACTIONS ON INSTRUMENTATION AND MEASUREMENT, and the *Journal of the Optical Society of America*. She has filed over 10 patents in LiDAR system and application. Her current research interests include LiDAR system and application.

JUNEN YAO is the former Vice Director of the Academic Committee and also the Honorary Director of the Key Laboratory of Micro-Nano Measurement Manipulation and Physics, Ministry of Education, Beihang University, where he is currently a Professor and a Ph.D. Supervisor with the School of Physics and Nuclear Energy Engineering and the School of Instrumentation Science and Opto-electronics Engineering. He is a member of the Chinese Academy of Engineering (elected in 2001).

He received the B.Sc. degree from the Dalian Institute of Technology (now known as Dalian University of Technology), Dalian, China, in 1952. He is one of the pioneers in the development and production of scanning tunneling microscope, transmission electron microscope, and scanning electron microscope in China. He has published over 140 papers and six books (including chapters in books). His research interests include nanotechnology, near-field optics, electron optics, electron microscopy, and instrumentation. He received the second prize of the National Science and Technology Progress Award and other ten national or ministry-level prizes.